Theor Appl Climatol (2016) 124:1023–1031
DOI 10.1007/s00704-015-1449-3

ORIGINAL PAPER

Distribution of solar irradiance on inclined surfaces caused by moving clouds

Teolan Tomson [1]

Received: 6 December 2014 / Accepted: 30 March 2015 / Published online: 29 April 2015

Abstract The distribution of solar irradiance in shadows of discrete (broken) clouds differs from the distribution calculated for inclined surfaces on the basis of traditional transposition models and changes fast. This phenomenon is studied in this paper. For calculations of dynamic distributions of irradiance on inclined surfaces, a formal point source of direct radiation near the real position of the sun is defined as the source of the "imaginable radiation." This notion is used to create a one-dimensional (1D) simulation model, which allows the fast-changing distribution of irradiance to be calculated. In general, the coincidence of calculated and measured irradiance on inclined surfaces is good. The paper also shows how the current value of the diffuse component of solar radiation can be derived from measurements of total radiation in four differently tilted planes.

Nomenclature

Symbols

A	Albedo
G_0	Global irradiance on horizontal plane
G_B	Total irradiance on vertical plane due shadow
G_F	Total irradiance on vertical plane due sun
G_d	Diffuse component of the irradiance
G_{d0}	Diffuse component of the irradiance on horizontal plane
G_{dB}	Diffuse component of the irradiance on vertical plane due shadow
G_{dF}	Diffuse component of the irradiance on vertical plane due sun
G_p	Total imaginable irradiance
G_{p0}	Global imaginable irradiance on horizontal plane
G_{pT}	Direct irradiance on tilted plane calculated from imaginable radiation
G_r	Ground-reflected irradiance
G_T	Total irradiance on tilted plane
Θ_T	Incident angle for the real position of the sun
Θ_{Tp}	Incident angle for the fictive (imaginable) position of the sun
α_p	Height (elevation) angle of the imaginable point source of direct radiation
α_s	Height (elevation) angle of the sun
β	Tilt angle
$\Delta\alpha_p$	Angle shift between α_p and α_s
γ	Relative azimuth angle
γ_s	Azimuth angle of the sun

Symbols marked with asterisk "*" denote their relative to G_0 value, which is the ratio of any optional irradiance vs global irradiance.

For instance $G^*_{d0}=G_d/G_0$ is relative value of diffuse component on the horizontal plane, etc.

1 Introduction

Fast dynamic processes of solar radiation are caused by shadows of discrete, mainly *cumulus*, clouds: *Cumulus humilis* (Ch), *Cumulus mediocris* (Cm), and *Cumulus fractus* (Cf). Stochastic values of irradiance (on the horizontal plane) and its transients have been analyzed (Tomson 2010, 2014; Tomson and Hansen 2011), but moving clouds also involve different distribution laws on inclined surfaces, which are used

✉ Teolan Tomson
Teolan.Tomson@ttu.ee

[1] Department of Materials Science, Tallinn University of Technology, Ehitajate tee 5, 19086 Tallinn, Estonia

in solar technology, that is, PV electricity generation and production of domestic hot water. Therefore, this phenomenon should have some importance and it is analyzed in the present study.

Regular solar radiation measurements and databases of solar irradiance have usually used recordings of beam radiation G_b, diffuse radiation G_{d0} on the horizontal plane, and radiation reflected from the ground G_r (McArthur 2005). Here and below, solar radiation is expressed via its irradiance G. Global radiation on the horizontal plane G_0 and total radiation on the plane of any optionally tilted plane G_T have to be found using recalculations.

Several transposition models have been developed for the recalculation. The fundamental law was proposed by Liu and Jordan (1963) and is still in use; significant development was achieved by Ineichen et al. (1990), who also considered radiation reflected from the ground. Overviews of such transposition models can be best found in books such as Perez et al. (2001), Muneer (2004), and Duffie and Beckman (2006). These models consider the static character of solar radiation using its averaged values and do not describe dynamic effects on inclined surfaces.

2 One-dimensional model of relative irradiance for the vertical profile along the sun's azimuth

On observing the simultaneous irradiance in alternating shadows of clouds on differently tilted surfaces as shown in Fig. 1 (Tomson 2013), the non-uniform character of its distribution and frequent changes have to be underlined. The numbers in the legend of Fig. 1 are the "addresses" of the said distributions on the relative time-scale in seconds. They appear randomly. F is the averaged distribution for the whole packet.

To attempt to explain such behavior, a one-dimensional (1D) simulation model along the sun's azimuth γ_s is proposed.

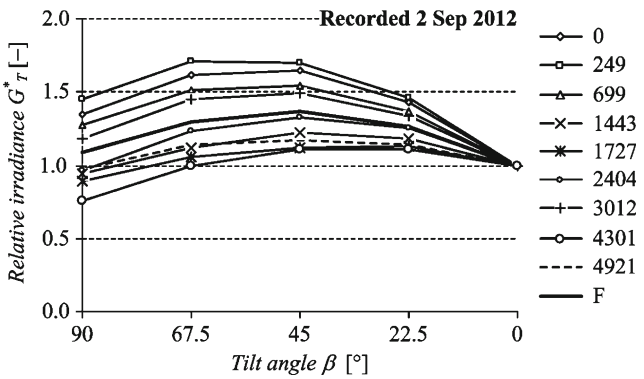

Fig. 1 Relative solar irradiance on inclined surfaces, recorded in the shadows of *Cumulus fractus* clouds, which is a random function of relative time instants (presented by seconds)

The proposed model is an explication of the Liu and Jordan model suited for a study of dynamic processes. The proposed model requires some hypothetical assumptions: diffuse radiation and radiation reflected from the ground are considered to be isotropic; direct radiation is expected to be emitted from a single source although really it may be emitted from several sparse (thin) sites in non-uniform clouds.

Existing non-isotropy is considered via an imaginable point source of radiation with coordinates α_p,γ_p somewhere near the actual position of the sun with the coordinates α_s,γ_s. Radiation emitted from that source has irradiance G_p, which has the character of direct radiation with a corrected incident angle Θ_{Tp} (α_p,γ_p), Fig. 2, and magnitude, which can be calculated via the declared and measured initial data (Appendix).

In Fig. 2, the symbol Θ_z is the zenith angle, β is the tilt angle of the receiver plane, and S(0)… S(180) are sensors (pyranometers). The number in brackets shows their tilt angle.

In clear-sky conditions $\alpha_p \rightarrow \alpha_s$, but in a general case, $\alpha_p = \alpha_s \pm \Delta\alpha_p$, where $\Delta\alpha_p$ varies randomly. This phenomenon is probably caused by invisible direct radiation from the sun ($\lambda > 800$ nm), which is able to shine through sparse (thin) sites in clouds and, to a lesser degree, by reflected radiation from the edges of clouds. Clouds and these sites are moving continuously and therefore G_p and α_p are variable. As Ch, Cm, and Cf clouds in the summer season appear mostly around noon (Tomson 2010), the value of α_s is mostly in the range of 30°–50° (at ~60° N) and $\Delta\alpha_p$ has finite values. According to the definition, small fluctuations of γ_p around the sun's azimuth $\Delta\gamma_s \rightarrow 0$ do not influence the value of G_{pT}. Possible fluctuations of G_{pT} due to fluctuations of the sun's imaginable azimuth are lost on the background of instrumental, installation, and sampling errors. G_0 is the global radiation on the horizontal plane comprising its components: direct radiation G_{p0} and diffuse radiation G_{d0}, G_F is the (total) radiation on the illuminated vertical plane, G_B is the (total) radiation on the shaded vertical plane, and G_r is the pure reflected radiation on the reverse horizontal plane. Its relative value is equal to albedo, $G^*_r = A$. In the conditions of high latitudes (~60° N), the sensors S(−90) and S(180) are always in shadow. Therefore, G_B has a diffuse origin, and according to the hypothesis proposed, it is a component of G_F too.

The imaginable (direct) component of radiation on the sensors S(90) and S(0) is a function of their incident angles if $G_p > 0$ exists, and conversely, the value of G_p can be calculated from known values of G_0 and G_F, as shown in the Appendix.

The analysis in the Appendix will be done in relative units marked with an asterisk, $G^* = G/G_0$, where $G \in \{G_B, G_F, G_r, \text{and } G_T\}$. Calculation of any real radiation regime is simple when the rates in relative units are known. A

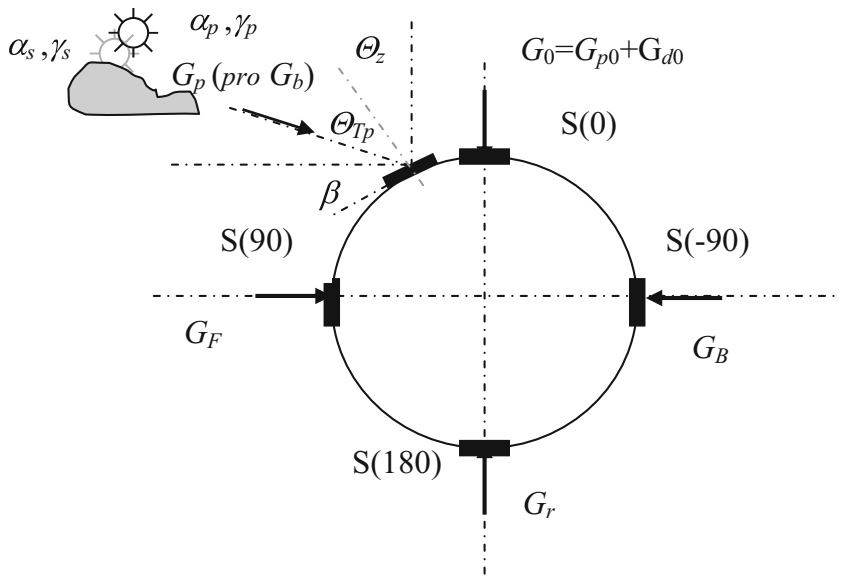

Fig. 2 Layout of symbols used in the proposed 1D model. Definitions are shown in the nomenclature of symbols and *numbers in brackets* show the tilt angle of corresponding sensors (*S*)

flow diagram of the proposed recalculation model is shown in the Appendix too.

In clear-sky conditions, α_p should be equal to α_s, but due to (instrumental and installation) errors, $\alpha_p \neq \alpha_s$ and a finite angle shift $\Delta\alpha_p$ with a value of a few degrees always exists.

In dark overcast conditions with $G_0 \approx 100$ Wm^{-2}, $G^*_F = G^*_B$, and therefore (according to Eq. (3) in the Appendix), $\tan[(1-G^*_{d0})/(G^*_F - G^*_B)] \to \propto$, which means that $\alpha_p \to 90°$. In dark (overcast) conditions, according to the created 1D model, direct solar radiation is formally emitted from the zenith point, although its value degenerates to zero.

According to Eqs. (5) and (6) in the Appendix, direct radiation degenerates to zero also at azimuths perpendicular to the sun's one ($\gamma \to \pm 90°$), and therefore, these profiles correspond to profiles assessed by pure diffuse (and reflected) radiation.

The proposed 1D model is useful due to the possibility of describing dynamical processes on inclined surfaces (which is an advantage), but it requires especial measurements of the total radiation, and public actinometrical datasets cannot be used (which is a disadvantage).

3 Hardware used for observations

Figure 3 shows the portable measuring stand used in the study, which has five sensors, S(0) … S(180). In the summer season of 2014, over 30 profiles (diagrams of the distribution) of the relative irradiance on tilted planes G^*_T were recorded with a sampling interval of 1 s. The azimuths of recording were fixed manually, and each particular recording lasted 10–20 s; also, the full "season" lasted ~5 min. In case of reduced measurements, only azimuths of 0°, 180°, and ±22.5° were controlled. According to Tomson (2014), the correlation time of diffuse radiation in conditions of alternating clouds is of the order of 5–15 min, which means that significant errors cannot be made in the time-delay measuring G_B and G_F separately.

Observations were made mainly at the former and recultivated landfill hill of Tallinn city at 59.36° N, 24.65° E, which is covered by grass.

In the measurements made in 2012 (Fig. 1), other combinations of sensors S(0), S(22.5) … S(90) (over 15 recorded G^*_T profiles) were used. Some of these results are used in the present study too. The sensors used during the whole study were photoelectrical pyranometers manufactured in Denmark

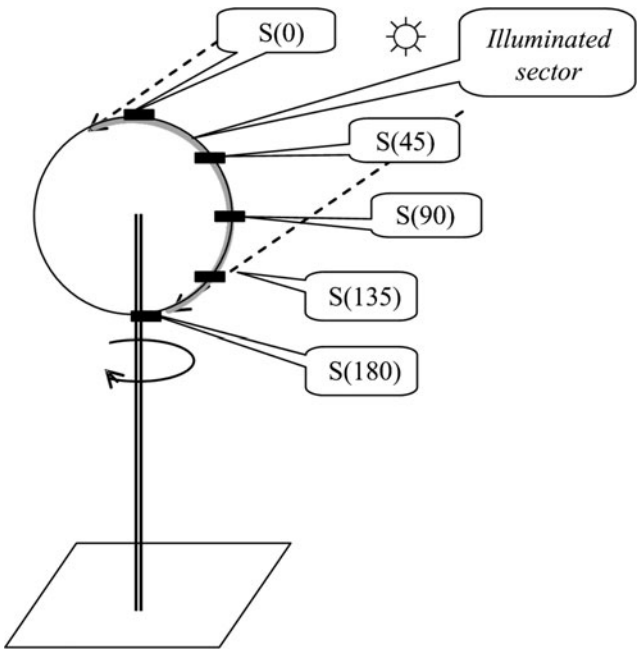

Fig. 3 The portable measuring stand used in the study. Tilt angles $\beta \in \{0 \ldots 180°\}$ of sensors (*S*) are fixed for each season. The ring with a sensor was rotated manually for different relative azimuths $\gamma \in \{0, \ldots 360°\}$

(Soldata 2015), which have a transient time of microseconds and allow the dynamic behavior of radiation to be studied. Their total uncertainty is 3 %. Data were saved on a midi LOGGER GL-200 datalogger. The sampling step used was 45° (22.5° in 2012) in the vertical plane and 22.5° in the horizontal plane. The irradiance was studied in the conditions of clear sky, overcast sky, and discrete clouds. In the last case, irradiance in shadows and sunny windows between clouds were studied. Under clouds, irradiance was always recorded without visible (to the human eye) shadows of any object over the ground. The distributions of irradiance on inclined surfaces under clear-sky conditions and in sunny windows between clouds have no essential difference (Figs. 4 and 5).

4 Distribution of irradiance in the vertical profile along the sun's azimuth

The validity of the composed 1D simulation model was controlled via several recordings presented in this section. The model describes the correct principal character of every individual recording, and in the majority of cases, the coincidence with the actual recording is good. The reliability of the simulation is analyzed in the next section.

When evaluating these diagrams, it must be taken into account that the calculation step was 22.5° but the step of actual measurements was 45°, and its values at 22.5°, 67.5°… 157.5° were found as interpolated values.

The diagram shown in Fig. 4 has a clear maximum point $G^*_T(-45^o)\approx 1.65$ and a concave character in the range $0>\beta>-90°$, where $G^*_T(-45^o)\approx 0.13$. For these recordings, the coordinates of the sun are $\alpha_s=37.6°$ and $\gamma_s=132.1°$, and the calculated value of α_p is 35°. The difference between the azimuths α_s and α_p is probably caused by reflections from clouds (and/or instrumental and installation errors). The sector

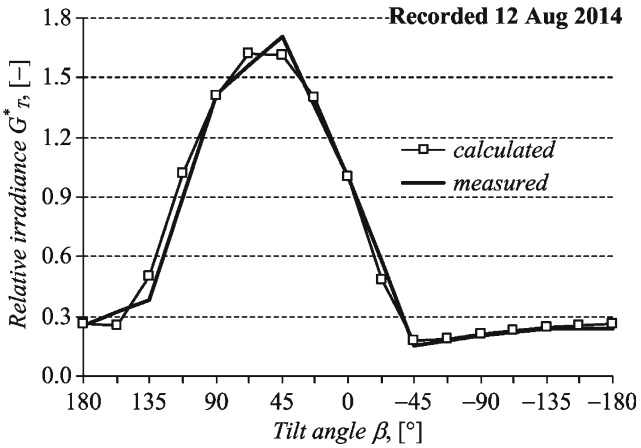

Fig. 4 Distribution diagram of the relative irradiance on differently inclined surfaces. The diagram corresponds to a large clear-sky window at global irradiance of 588 Wm^{-2} along the relative azimuth $\gamma=0°$

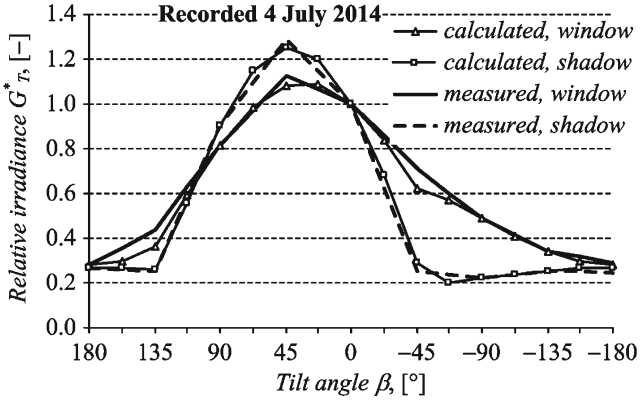

Fig. 5 Distribution of measured and calculated relative irradiance on inclined surfaces in conditions of changing global radiation along the relative azimuth $\gamma=0°$ in a narrow window between moving discrete clouds

$127°>\beta>-53°$ is illuminated. In clear-sky conditions, the level of diffuse radiation is low, and therefore, $G^*_T(-45°)$ on the shadow side is low too. The derivative $dG^*_T/d\beta$ has no certain sign and has both positive and negative values.

Figure 5 shows a diagram which demonstrates the dynamics of solar radiation due to the movement of discrete clouds.

First, the distribution of the irradiance in shadow was recorded. Two minutes later, the irradiance in sunshine was recorded. The characters of these two distribution diagrams differ distinctly, but diagrams recorded and calculated for the narrow sunny window are similar to that shown for a large window in Fig. 4. In this case, $\alpha_s=50.1°$ and azimuth $\gamma_s=145.8°$. Elevation angle of the imaginable point source depends on the illumination: in shadow $\alpha_p=42.6°$, but in the sunny window, it is $\alpha_p=50.5°$ ($\approx\alpha_s°$).

Figure 6 shows the vertical profile under a dark overcast sky at $G_0=110$ Wm^{-2}.

Here, G^*_T is monotonically decreasing while the tilt angle is increasing to both negative and positive tilt angles. In this case, the derivative is always negative: $dG^*_T/d\beta<0$. Figure 6 corresponds to $\alpha_s=32.8°$, $\gamma_s=133.2°$, and $\alpha_p=88°$.

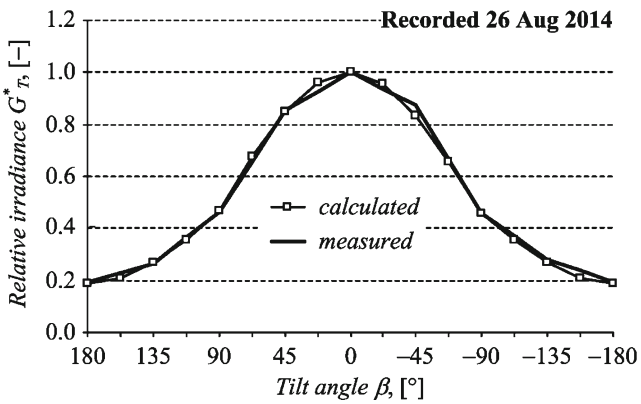

Fig. 6 Distribution of measured and calculated relative irradiance on inclined surfaces under thick cloud cover at a global irradiance of 110 Wm^{-2} along the relative azimuth $\gamma=0°$

5 Reliability of the 1D model

The reliability analysis of the composed 1D simulation model is summarized in Table 1, where the first column shows the date of the measurement, the second column the sun's elevation angle, the third column the shift in angle between the sun's real and imaginable elevations, the fourth column the average global irradiance, and the next nine columns the difference between the measured M and calculated C values of $G^*_T(\beta)$ at corresponding tilt angles β.

The results for three tilt angles (135°, 45°, and −45°) require comments. At 135°, the error has a relatively high value and the highest standard deviation among the results. This circumstance is the result of quantization: the edges of the illuminated sector are continuous variables, but the model uses a discrete sample interval ($\Delta\beta$=22.5° according to the analysis done), and a quantizing error is unavoidable. At 45°, the error is highest but the standard deviation has a moderate value. This circumstance refers to the systematic ~5 % error of the model in calculating the maximum point of $G^*_T(\beta)$. At −45°, depending on the current elevation angle of sun, the

Table 1 Reliability analysis of the composed 1D simulation model, which shows difference between calculated C and measured M values of relative irradiance on differently inclined surfaces, [%]

YYMMDD	α_s, °	$\Delta\alpha_p$, °	G_0, Wm^{-2}	$\Delta G^*_T(\beta)$, %								
				180	135	90	45	0	−45	−90	−135	−180
140503	46.07	6.41	377.8	0.23	12.13	−8.96	−5.34	−0.03	−4.02	−3.00	−0.52	0.00
140522	41.18	−1.71	631.6	0.35	−9.02	−0.07	−0.12	−0.08	7.06	0.03	2.68	1.69
140523	50.95	−22.88	114	0.12	−13.30	−0.37	4.78	−0.05	−2.54	−0.22	−0.37	−1.17
140523	50.4	−2.20	722.7	−0.39	2.04	0.40	−0.46	−0.06	3.80	0.15	−4.50	0.08
140523	49.8	−23.89	157.4	−0.08	−16.22	0.45	3.18	−0.06	−4.97	0.23	−0.26	1.92
140524	42.48	−13.08	636.8	−0.48	−32.72	0.49	10.82	−0.06	−38.42	−20.38	−12.31	−0.89
140526	42.22	−3.15	637.2	0.21	−10.08	−0.09	2.61	−0.08	5.66	0.22	3.09	0.81
140601	49.03	−14.18	239	0.30	−0.29	−0.43	4.40	−0.04	1.04	−0.25	3.62	1.16
140601	49.86	−24.93	187.1	−0.87	−10.56	0.35	8.08	−0.06	−6.73	−0.15	4.16	0.82
140603	46.84	40.15	172.6	0.20	−1.72	−0.01	−0.51	0.00	0.19	0.19	−2.88	0.54
140615	45.71	−6.46	209.9	−6.85	−17.95	0.51	5.40	−0.07	5.67	0.36	−5.48	0.02
140615	48.85	−7.66	138.7	0.00	−11.56	−0.01	4.51	−0.06	15.28	4.83	−5.61	0.00
140620	52.3	4.31	447.9	0.13	13.95	0.31	0.91	−0.02	4.87	0.27	−1.66	0.10
140621	42.27	−0.92	212.9	0.13	15.60	−0.42	4.06	−0.04	12.55	0.34	8.22	0.45
140621	43.7	−12.17	162	0.84	5.55	0.44	2.30	−0.04	7.09	0.41	2.62	−0.30
140702	44.88	−2.07	736.7	0.06	−3.02	0.17	2.53	−0.08	−2.80	−0.43	−0.59	−1.10
140704	50.6	−7.98	220	−0.14	7.82	−0.01	4.54	−0.03	9.30	0.25	0.09	0.80
140704	50.6	−0.09	862.7	−0.35	−0.92	0.11	3.62	−0.05	−4.00	0.20	−0.64	−2.21
140705	46.35	−2.46	756.2	0.22	−1.28	0.16	3.89	−0.06	−1.64	0.37	1.25	−0.30
140707	53.17	−5.75	238.8	−0.32	0.12	−0.43	8.47	−0.03	13.56	0.17	−3.63	0.02
140707	53.17	2.81	238.8	0.39	0.03	0.03	1.95	−0.04	−6.32	0.44	0.21	1.21
140714	37.23	−11.21	183.2	0.00	−6.50	−0.05	4.98	−0.07	−3.49	0.15	1.57	1.80
140714	37.23	0.49	183.2	0.00	11.14	−0.15	1.79	−0.06	9.35	0.09	0.58	0.72
140727	48.97	−0.88	736.9	1.35	0.41	0.05	3.78	−0.06	−5.40	0.40	0.84	−2.00
140808	39.12	−1.28	671.2	1.40	−12.96	0.31	8.79	−0.08	−0.63	−0.21	−2.67	−4.08
140808	39.58	37.89	178.5	−0.07	−2.80	−0.33	7.70	0.00	−2.69	−0.45	−1.14	−0.98
140810	43.67	−3.43	628.4	2.93	−5.05	−0.28	7.87	−0.08	−1.68	−0.44	−1.54	−2.70
140812	37.62	−2.63	588.1	−0.20	−11.63	0.56	9.13	−0.10	−2.09	−0.40	−0.73	−1.81
140812	38.27	−5.63	130	−0.06	−6.50	−0.44	11.64	−0.05	2.40	−0.36	−1.51	−0.83
140812	42.61	10.09	159.7	1.82	6.90	4.39	1.52	−0.01	4.23	3.79	2.40	1.82
Aver (M-C), %				0.03	*−3.28*	−0.11	*4.23*	−0.05	0.49	−0.45	−0.49	−0.15
Stdev (M-C); %				1.50	*10.55*	1.87	3.71	0.02	*9.58*	3.98	3.70	1.43

sensor S(−90) may be in shadow or (lightly) illuminated, which results in an increased standard deviation.

For other optional points of $G^*_T(\beta)$, the error has a low value of ~1 %. The difference between errors at +180° and −180° (less than 1 %) lies within the margin of instrumental errors.

Analysis of the calculated elevation of the imaginable point source should be of interest too. From the analysis of Table 1, a weak (0.7 % slope of the trend line) negative correlation of the difference $\Delta\alpha_p=\alpha_p-\alpha_s$ with the global radiation G_0 can be found (Fig. 7). High values of G_0 involve low values of $\Delta\alpha_p$. In most cases, $\Delta\alpha_p<0$, which means that the fictive source of imaginable radiation mostly lies below the sun's real position. At a low value of global radiation, $G_0<200$ Wm^{-2}, the standard deviation of $\Delta\alpha_p$ is high (over 25°), which is the result of instrumental and installation errors, which influence $\Delta\alpha_p$ significantly at low values of global radiation. The installation error is a result of the inadequacy of the sensors' real positions with respect to their ideal positions. Installation of the portable stand on rugged grassland always results in a finite leveling error.

6 Distribution of irradiance in space

The experimental distribution of the relative irradiance in space and the total irradiance on inclined planes $G^*_T(\beta\,\gamma)$ is shown in Figs. 8, 9, and 10. Here, γ is the azimuth of a vertical plane in which the irradiance is recorded relative to the solar azimuth γ_s.

Figure 8 shows the spatial distribution under overcast clouds. This distribution is invariant to the direction, and its profile along the sun's azimuth γ_s is shown in Fig. 6. A similar distribution is valid for a shadow of a thick discrete cloud at the low value of $G_0<200$ Wm^{-2} too.

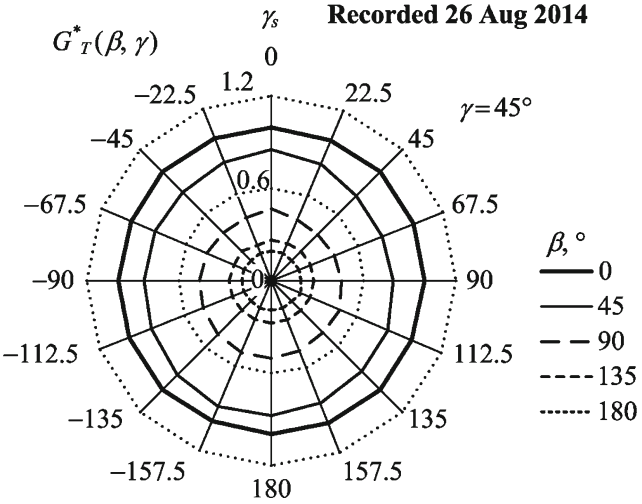

Fig. 8 Spatial distribution diagram of the total irradiance on inclined planes $G^*_T(\beta,\gamma)$ in overcast conditions at a global irradiance of G_0= 110 Wm^{-2} depending on direction and tilt angle

Figure 9 shows the distribution of $G^*_T(\beta,\gamma)$ in a large sunny window at $G_0=588$ Wm^{-2} between discrete clouds, which is symmetric for the 0°/180° axis. A similar form of the diagram is valid for any clear-sky recording. The direction $\gamma=0$ coincides with the solar azimuth $\gamma_s=132.1°$, and its profile is shown in Fig. 4.

Figure 10 shows the distribution of $G^*_T(\beta\,\gamma)$ under sparse (thin uneven) overcast clouds at $G_0\approx400$ Wm^{-2}, which is

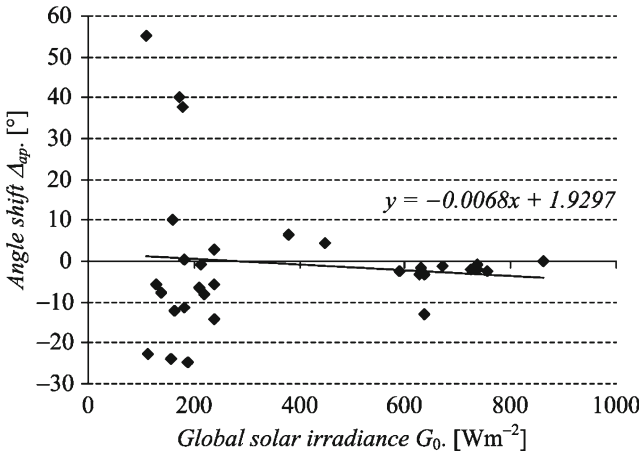

Fig. 7 Correlation diagram between angle shifts of the imaginable point source $\Delta\alpha_p$ versus global irradiance G_0

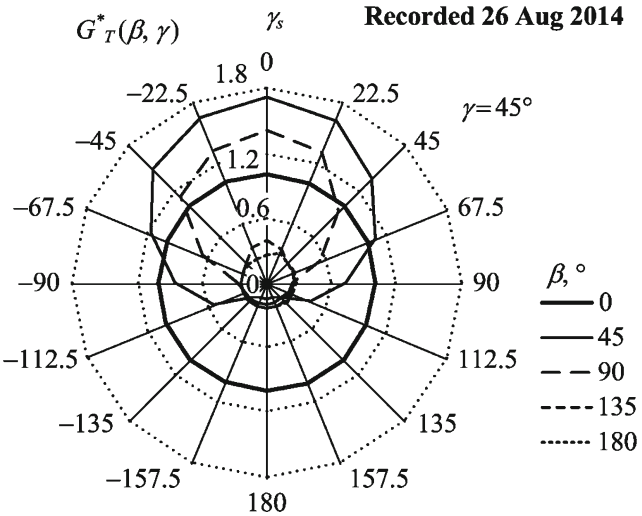

Fig. 9 Spatial distribution diagram of the total irradiance on inclined planes $G^*_T(\beta,\gamma)$ in conditions of a large sunny window between clouds at a global irradiance of 588 Wm^{-2}

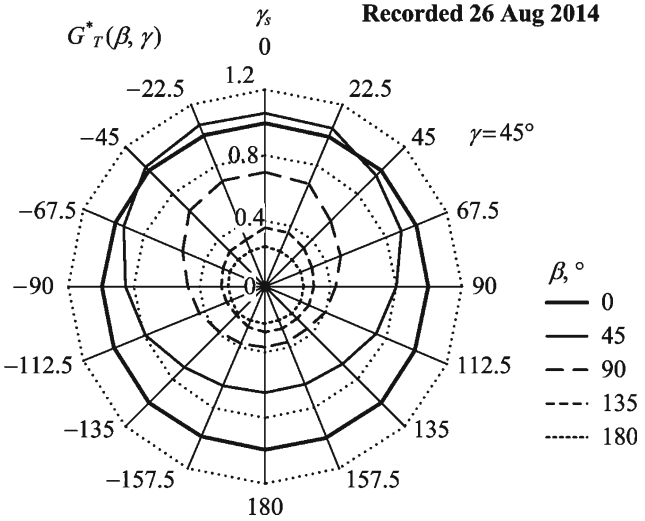

Fig. 10 Spatial distribution diagram of the total irradiance on inclined planes G^*_T (β,γ) under sparse overcast clouds at global irradiance of ~400 Wm^{-2}. The diagram is symmetric for the 0°/180° axis

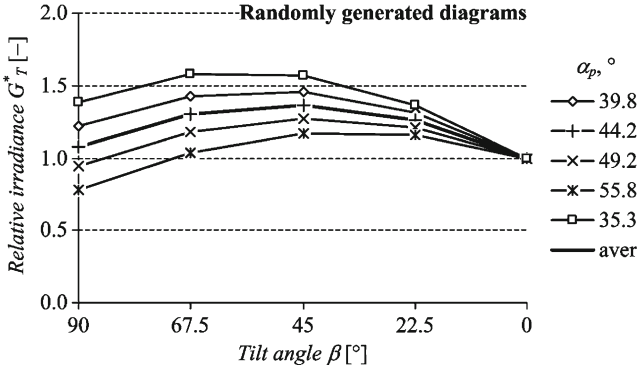

Fig. 11 Artificial distribution of solar irradiance on inclined surfaces generated at a random elevation angle of the imaginable point radiation in the range of 30°<α_p<60°

symmetric for the 0°/180° axis but has a clear maximum due to sun (γ=0°). Here, α_s=43.7°, γ_s=162°, and α_p=56°.

Similarly to Fig. 10, the diagrams are characteristic for recordings in shadows under most discrete *cumulus* (Ch, Cm, and Cf) clouds. Analysis of the recorded data shows that in 85 % of cases, the azimuth of imaginable radiation cannot be discriminated from the sun's azimuth, while in 15 % of cases it may be different, but the deflection lies within the range of possible errors (including errors due to the sampling step of 22.5°). The noted quality of imaginable radiation motivated the usage of a 1D model to describe the vertical profile of solar radiation mainly along the sun's azimuth, where a point source of imaginable radiation with a height angle α_p fluctuates up and down around the sun's height angle α_s.

7 Usage of 1D simulation model

Figure 11 shows a small packet of distribution diagrams artificially generated with the 1D simulation model using randomly generated height angles of an imaginable radiation source in the range of 30°<α_p<60°.

The numbers in the legend show values of α_p, which are presented in order of their appearance. The bold average line "aver" coincides with the case α_p=44.2°.

Comparison of Fig. 11 with Fig. 1 shows the lack of principal differences, and in such a way, the natural phenomenon can be reproduced artificially. The artificial G^*_T may be useful for the précised (most exact) calculations of solar energy if the statistics of sunny windows versus cloud shadows are known.

8 Summary

The present study highlights the dynamic behavior of the solar radiation mainly in conditions of moving discrete clouds. Shadows of clouds quantify the value of irradiance and involve its different distribution on inclined surfaces. To describe such dynamic behavior, an imaginable but effective notion of a "point source of direct radiation" can be used. For the calculation of this distribution, a 1D calculation model has been proposed which shows a good coincidence with measured recordings. It is also shown how the current value of the diffuse component of solar radiation can be derived from measurements of global radiation and total radiation on three differently tilted planes.

Appendix

One-dimensional simulation model, described by flow diagram below is created using relative units marked with an asterisk $G^*=G/G_0$, where $G\in\{G_0, G_B, G_F, G_r,$ and $G_T\}$. All symbols are declared in the nomenclature. Building the model for the vertical profile along the sun's azimuth, a simple relation is valid $\Theta_{Tp}=\pi/2-(\alpha_p+\beta)$. According to the isotropic sky model (Quashning and Hanitch 1998),

$$G^*_B = \mathrm{A} \times (1-\cos\beta)/2 + G_{d0} \times (1+\cos\beta)/2 \qquad (1)$$

Considering that at β=−90°, its cosine is zero, cos β=0, which results in

$$G^*_{d0} = 2 \times G^*_B - A \quad (2)$$

Imaginable (direct) component of radiation on the sensors S(90) and S(0) can be calculated from G_p according to their incident angles if G_p>0 exists. Also backward – value of G_p can be calculated from known values of G_0 and G_F, what is shown below.

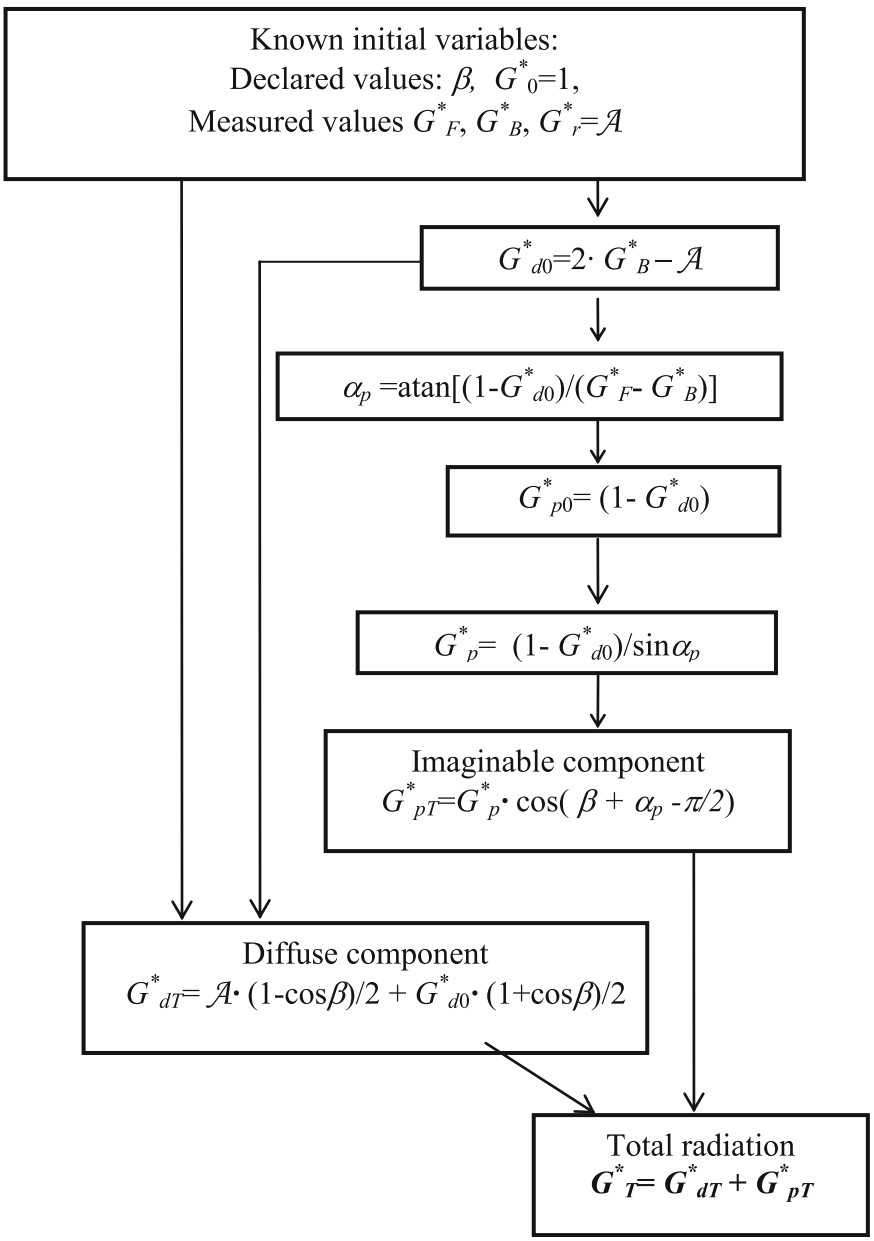

Flow diagram of calculations of the proposed 1D simulation model.

The diffuse component on the illuminated vertical plane is equal to that in shadow $G^*_{dF}=G^*_{dB}=G^*_B$. The relative total

radiation on the illuminated vertical plane is $G^*_F = G^*_B + G^*_p \times \cos\Theta_{Tp}$ and that on the horizontal plane is $G^*_{p0} = G^*_p \times \sin\alpha_p == 1 - G^*_{d0}$, from which the following equation can be expressed:

$$a_p = \text{atan}\left[\left(1 - G^*_{d0}\right)/\left(G^*_F - G^*_B\right)\right] \tag{3}$$

and

$$G^*_p = \left(1 - G^*_{d0}\right)/\sin\alpha_p \tag{4}$$

Imaginable component on an optionally declined plane can be calculated

$$G^*_{pT} = G^*_p \times \cos\left(\beta + \alpha_p - \pi/2\right) \tag{5}$$

Total radiation (irradiance) on an optionally declined plane is sum of diffuse (1) and imaginable (5) components

$$G^*_T = G^*_{dT} + G^*_{pT} \tag{6}$$

If the relative irradiance on a tilted plane different from the sun's azimuth $G^*_T(\gamma)$ has to be found, then Eq. (6) should be used:

$$G^*_{pT}(\gamma) = G^*_{pT} \times \cos\gamma \tag{7}$$

Using Eq. (5), $G^*_{pT} \geq 0$ always has positive (or zero) values.

References

Duffie JA, Beckman WA (2006) Solar engineering of thermal processes, 3rd edn. Wiley, NY

Ineichen P, Guisan O, Perez R (1990) Ground-reflected radiation and albedo. Sol Energy 44(4):207–214

Liu BYH, Jordan C (1963) The long-term average performance of flat-plate solar energy collectors: with design data for the US, its outlying possessions and Canada. Sol Energy 7:53–74

McArthur LJB (2005) Baseline Surface Radiation Network (BSRN) operations manual. WMO/TD-No 1274

Muneer T (2004) Solar radiation and daylight models, 2nd edn. Elsevier, Butterworth-Heinemann

Perez R, Aguiar R, Collares-Pereira M, Dumortier D, Estrada-Cajigal V, Gueymard C, Ineichen P, Littlefair P, Lund H, Michalsky J, Olseth JA, Renne D, Rymes M, Skartveit A, Vignola F, Zelenka A (2001) Resource assessment: a review. In: Gordon J (ed) Solar energy. The State of the Art. James & James, London, pp 497–575

Quashning V, Hanitch R (1998) Irradiance calculations on shaded surfaces. Sol Energy 62(5):369–375

Soldata Instruments, 2015. www.soldata.dk

Tomson T (2010) Fast dynamic processes of solar radiation. Sol Energy 84(2):318–323

Tomson T (2013) Diffuse radiation in Estonia. TEUK-XV, Proc. 15th Conf. Study and Usage of Renewable Energy Sources, EMU, Tartu, pp. 86–95

Tomson T (2014) Dynamic behaviour of diffuse solar radiation. Theor Appl Climatol 117:399–402

Tomson T and Hansen M (2011) Dynamic properties of *clouds Cumulus humilis* and *Cumulus fractus* extracted by solar radiation measurements. Theoreticl and Aplied Climatology vol.106, n#1-2, 171–172